Impact of Phosphorylation on alpha-Synuclein Structural Determinants

Anton Emil Dorn,[†,‡] Emile de Bruyn,[†,¶,‡] Giulia Rossetti,[*,¶,§,‖] Claudio Fernandez,[⊥,#] Tiago F. Outeiro,[@,△,▽] Jörg B. Schulz,[‡,‖,††] and Paolo Carloni[‡,§]

† *Equally contributed to this work*

‡ *Department of Physics, RWTH Aachen University, 52062 Aachen, Germany*

¶ *Jülich Supercomputing Centre (JSC), Forschungszentrum Jülich GmbH, 52425 Jülich, Germany*

§ *Computational Biomedicine (IAS-5/INM-9), Forschungszentrum Jülich GmbH, 52425 Jülich, Germany*

‖ *Department of Neurology, RWTH Aachen University, 52074 Aachen, Germany*

⊥ *Max Planck Laboratory for Structural Biology, Chemistry and Molecular Biophysics of Rosario (MPLbioR, UNR-MPINAT). Partner of the Max Planck Institue for Biophysical Chemistry (MPINAT, MPG). Centro de Estudios Interdisciplinarios, Universidad Nacional de Rosario, S2002LRK Rosario, Argentina*

Department of NMR-based Structural Biology, Max Planck Institute for Multidisciplinary Sciences, 37077 Göttingen, Germany

@ *Department of Experimental Neurodegeneration, Center for Biostructural Imaging of Neurodegeneration, University Medical Center Göttingen, 37075 Göttingen, Germany*

△ *Max Planck Institute for Multidisciplinary Sciences, 37075 Göttingen, Germany*

▽ *Translational and Clinical Research Institute, Newcastle University, Newcastle upon Tyne NE1 7RU, United Kingdom*

†† *JARA Brain Institute Molecular Neuroscience and Neuroimaging (INM-11), Research Centre Jülich and RWTH Aachen University, 52074 Aachen, Germany*

Received March 23, 2023; E-mail: g.rossetti@fz-juelich.de

Abstract: Serine 129 and, to a lesser extent, serine 87 can appear phosphorylated in the intrinsically disordered protein human α-synuclein (AS), a key player in Parkinson's disease, where it accumulates in proteinaceous aggregates. Intriguingly, both phosphorylations are located in a highly negative potential region of the protein. Here we used molecular simulation to provide insight in the selective phosphorylation by polo-like kinase 2 (PLK2), in both monomeric and fibrillar forms of AS. We suggest that phosphorylation does not impact on the structural determinants of the physiological AS conformational ensemble, as the phosphate group is mostly solvated. Our findings are consistent with experimental data on the non-acetylated, non-physiological form of the protein. The phosphate groups of pAS may be solvated also in the aggregated form.

1. Introduction. Parkinson's disease (PD) is the second most common neurodegenerative disease after Alzheimer's disease,[1] affecting several million people worldwide.[2,3] The typical pathological hallmark is the accumulation of fibrillar protein inclusions, know as Lewy bodies (LBs) and Lewy neurites (LNs) in the brain.[4,5] The major component of LBs and LNs are fibrillar forms of the human α-synuclein (AS) protein.[3,6] AS is a 140 amino acid 'disordered' conformational ensemble both in aqueous solution and in vivo.[7,1] In physiological conditions, the protein is acetylated on the first residue, although in vitro studies suggest this N-terminal acetylation does not significantly change the fibrillization propensity in vitro. In LBs, a significant fraction of AS is phosphorylated on serine 129.

However, it is still unclear whether this post-translational modification (PTM) plays a pathological and/or physiological role.[9–11] The formation of the Ser129-O-PO_3^{2-} group at the C-terminus (residues 96-140) is intriguing, because the latter is highly negatively charged (pAS) (Figure 1)[2]. The negatively charged C-term differs from the other two regions of the protein: the positively charged N-terminus (residues 1-60) and the overall neutral non-amyloid component (NAC) region (residues 61-95) (Figure 1). Its impact on the structural determinants is not known.[3]

```
MDVFMKGLSKAKEGVVAAAEKTKQGVAEAAGKTKE  35
GVLYVGSKTKEGVVHGVATVAEKTKEQVTNVGGAV  70
VTGVTAVAQKTVEGAGSIAAATGFVKKDQLGKNEE 105
GAPQEGILEDMPVDPDNEAYEMPSEEGYQDYEPEA 140
```

Figure 1. Sequence of amino acids in α-synuclein; positively charged residues are highlighted in blue and negatively charged ones in red.

Here, we used computational tools in an effort at addressing these important issues. First, we used electrostatic modeling to provide a rationale for the phosphorylation at the C-term by target kinases.[15] Next, we investigated the impact of the PTM on the protein in its monomeric form and in the fibrils. Our investigation on monomeric AS here builds upon our AMBER-based Replica Exchange with Solute Tempering 2 (REST2)[16] enhanced sampling predictions of wild-type[17,18] and mutants[18] of the conformational ensemble of AS monomer in aqueous solution, in its physiological form[19,4]. The calculations are based on the two force fields tailored for IDPs. These are the DES-Amber ff99SB[43]

[1] It acquires instead some degree of structure when bound to the membrane or to cellular partners.[8]

[2] Phosphorylation introduces as many as two negative charges in AS at physiological pH (the pKa_1 and pKa_2 of phosphoserine are <2 and 5.6[12]). However, it might be possible that in that negative potential the phosphate is monoprotonated (Ser129-O-PO_2OH^-, pASH). The effect of protonation is discussed in the Supplementary Information)

[3] The CD spectra of the *non-N-term acetylated*, non physiological form of the protein[13,14] in solution points to significant changes in the structural ensemble. However, the structure of the physiological form differs from that of the non-aceylated one, so conclusions cannot be made from these studies

[4] To the best of our knowledge, these are the only molecular simulation studies so far on AS' physiological form in explicit solvent.[5]

and the AMBER a99SB-*disp* force fields.[20] The latter has already been successfully used for the unacetylated form of the protein in the free form[20,44] and in the presence of ligands.[21] The conformational space of the protein was efficiently explored using the REST2 algorithm and it was shown to reproduce a variety of biophysical properties of the protein. However, the simulations presented here face the challenging doubly charged phosphate group. While the force field for phosphorylation (phosphorylated serine, threonine, and tyrosine) are present in the most widely used force fields, from AMBER[45] (DOI: 10.1007/s00894-005-0028-4) , to CHARMM[46,47] and to GROMOS[48] , and also even quite recently (https://doi.org/10.1021/acschemneuro.2c00611), some of these parametrizations (including that of AMBER) have at times shown artifacts.[49,50] Here, our caculations are based on (i) the standard a99SB-*disp* Amber forcefield[45] (DOI: 10.1007/s00894-005-0028-4) for the protein and the solvent, but with a specific, AMBER-compatibe parametrization of the phosphate group[51] and (ii) the DES-Amber force field, for which phosphate parameters have been calibrated based on osmotic coefficient calculations.[52]

2. Methods

Electrostatic modeling. The X-ray structures of the AS kinases PLK2, CK1, CK2, GRK5 and LRRK2 were taken from the Protein Data Bank[53] (IDs 4I5P,[54] 3UYS,[55] 1NA7,[56] 4TNB[57] and 6VNO[58] respectively). The binding site and active site location were identified using ProRule .[59,60] The sequence alignments in the area of the predicted binding site were performed using Clustal Omega.[61] Figure 2 in the SI shows that a common motif across all these enzymes can be found.

For monomeric AS, we considered the main representative conformer from a cluster analysis of the molecular simulations performed here (see below), present for 1.44 % of the simulation time. For the fibrils, we took the solid state structure (PDBid 2N0A).[62]

The surface potentials of the proteins along pAS and AS (in solution and in the aggregate forms) were calculated using the Poisson-Boltzmann equation using APBS and PDB2PQR[63] and visualized in PyMOL.[64]

Molecular simulations. The initial structure of the monomer best reproduced the chemical shifts for the first twelve residues in ref.[17] The phosphate group was added to Ser129 by editing the structure in PyMOL.[65]

The proteins were inserted in a water-filled dodecahedral simulation box with periodic boundary conditions and minimum distance of 3.5 nm between the protein and the box edges. Na^+ and Cl^- ions were added to neutralize the system and achieve a concentration of 150 mmol L^{-1}. Table 1 shows the composition of the systems, how many atoms and which type of them.

Table 1. Number of atoms in the simulation box for the three systems simulated here. The TIP4P-D water model uses a forth dummy atom to simulate water, thus the total number of atoms including dummy atoms is given in brackets.

	Protein	Water	Sodium	Chlorine
AS	2,020	190,533 (254,044)	186	176
pAS	2,023	172,359 (229,812)	171	159

The simulations were based on: (i) the a99SB-*disp* force field[20] together with a modified version of the TIP4P-D water model compatible with the force field; (ii) the DES-Amber force field[43] and the standard TIP4P-D water (See Table 20 in the SI for a full list of the parameters used). The proteins turned out not to be in contact with their images at distances 1.2 nm or lower during these simulations. Long range electrostatics were evaluated using the Particle-Mesh Ewald (PME) method,[66] using a cutoff distance of 1.2 nm in real space. Also the Van-der-Waals interactions featured the same cutoff.

Constant temperature conditions were achieved by coupling the systems with the Nose-Hoover thermostat[67] at 300 K and a time constant of 0.5 ps. Constant pressure was achieved with a Parrinello-Rahman barostats[68] at 1 bar and a time constant of 2 ps (Table 20). The LINCS algorithm was used for all bonds involving hydrogen atoms.[69] The equations of motions were integrated using the `md` leap-frog algorithm, with a timestep of 2 fs.

The proteins underwent an energy minimisation (Table 15 in the SI for details). The systems were then heated in the NVT ensemble from 0 K to 300 K in 1 ns (Table 17 in the SI). Finally, 100 ns REST2 simulations in the NVT ensemble were carried. We checked that the proteins are not in contact with their images at distances lower than 1.2 nm during any of these simulations.

A cluster analysis was carried out with the `gmx cluster` code in GROMACS.[70,71] A cutoff of 0.5 nm and the `linkage` method were chosen.

The following properties were calculated: (i) The radius of gyration R_g, calculated using the `gmx gyrate` module from GROMACS. (ii) The hydrodynamic radius, calculated from the radii of gyration using a linear fit proposed by Allison et al.[32] (iii) The NMR chemical shifts of the C_α atoms, calculated using `shiftx2`.[72] (iv) The secondary structure elements, calculated using the MDTraj[73] and DSSP[74] codes. (v) The CD spectra, using DichroCalc.[75] Only conformations after 12 ns were considered. Additionally the average of all used clusters weighted to their occurrence was calculated. (vi) The solvent accessible surface area (SASA) using the `gmx sasa` code from GROMACS. (vii) The contact map of the protein using the `gmx mdmat` code in GROMACS. (viii) Radial distribution functions (RDF) from the oxygen atoms of serine 129 using `trrdf` and `int_trrdf` using the SPEADI[76] code developed by the authors. (viii) Hydrogen bonds were defined by a distance between oxygen or nitrogen atoms with polar hydrogen below 0.3 nm, and an angle with the hydrogen-polar atoms between 160 and 180 degrees. To identify the hydrogen bonds VMD was used.[77] (ix) Salt bridges were defined by a distance between to charged atoms in the protein at a distance below 0.32 nm. The `pairdist` module from GROMACS was used.

3. Results and Discussion

Electrostatic modeling. Polo like kinase 2 (PLK2)[78,79] is thought to be the most important kinase phosphorylating AS on S129.[80] Previous work[81] and electrostatic modeling performed here shows that the cleft between the active and binding sites is positively charged (Figure 2). This is expected to steer the interaction with the negatively charged C-terminus (including S129), both in its monomeric, intrinsically disordered form (Figure 2(b)) and in the fibrils (Figure 2(c)), where the NAC region forms a stacked structure and the N-term and C-term.[6] PLK2 also phosphorylates S87, albeit at a lower extent.[82] Phosphorylation does not seem to occur at S42 and S9.[82] Notably, while S87 is still located in a negative potential region of the protein (albeit less negative than S129) in solution (Figure 2(b)) and in fibrillar

[6] An analysis of other kinases phosphorylating S129 is presented in the SI

forms (Figure 2(c)), the other two serine residues are located at the N-term, characterized by a more positive potential. Thus, we may expect an 'electrostatic steering' also for S87 but not for the other two, consistently with experimental evidence.

Molecular simulations of the monomer. We performed REST2 simulations[16] for 100 ns, using 32 replicas afor both AS and pAS monomers. Additionally 100 ns of MD were carried out. We performed simulations using both the the DES-Amber and the a99SB-*disp* force fields (for the latter we also investigated the protein with a monoprotonated phosphate (pASH). We report here the results for the first calculations, while the second can be found in the SI.

Convergence. We inspected: (i) the running averages of the percentage of residues featuring any secondary structure and in a helix structure (Figures 7 to 9 in the SI)), plotted as a function of the simulation time, reached a plateau after 12 ns of the simulation (see SI); (ii) the running averages of the chemical shifts of C_α (same Figures) which converge closely to the experimetnal values (Figure 10 in the SI) and (iii) the RMSD (Figure 13 in the SI). The use of the latter however has limitation as AS is an IDP.[83] . Based on this analysis, we calculated structural properties in the interval 12-100 ns.

Comparison with experimental data. The computational setup turns out to reproduce the available experimental data (NMR, CD and hydrodynamic radius)[84–86] available for AS (See SI).

Effect of phosphorylation. In Figure 3 the structures of the ten most representative structures of AS and pAS are offered. They were determined with clustering. Those ten structures make up 35 % and 33.7 % of the simulation time respectively for AS and pAS.

The calculated hydrodynamic radius R_H (Table 2) and the radius of gyration R_g decrease upon phosphorylation. However the SASA increases in the NAC region (Table 3).[7] The intramolecular interactions between the NAC region and the other regions slightly increase, as shown by the contact map (Figure 6). Accordingly, the intermolecular hydrogen bonds increase, within the caveat that it features a large standard deviation (Table 2). Consistently, the distribution of the number of such interactions show a wide normal distribution (Figure 17 in the SI).

These H-bonds are almost exclusively formed within every single domain (see Fig. 4).

The number of salt bridges increases upon phosphorylation. The most persistent salt bridges common to both forms involve the N-term and NAC regions (K23-E20 and K58-E61, respectively, see Figure 4). Please notice that given the disordered nature of IDPs intramolecular contacts are labile. Different salt bridges can form over longer time scales or at different starting points. Few salt bridges are formed between the C-terminus and one of the two other domains.

We conclude that the compactness of the AS conformational ensemble slightly increases upon phosphorylation, but maybe not in the NAC region. This is associated with a small increase of intramolecular interactions. This is what one may expect given an increase of negative charge at the C-terminus which can increase its interaction with the rest of the protein, and, particularly, with the positively charged

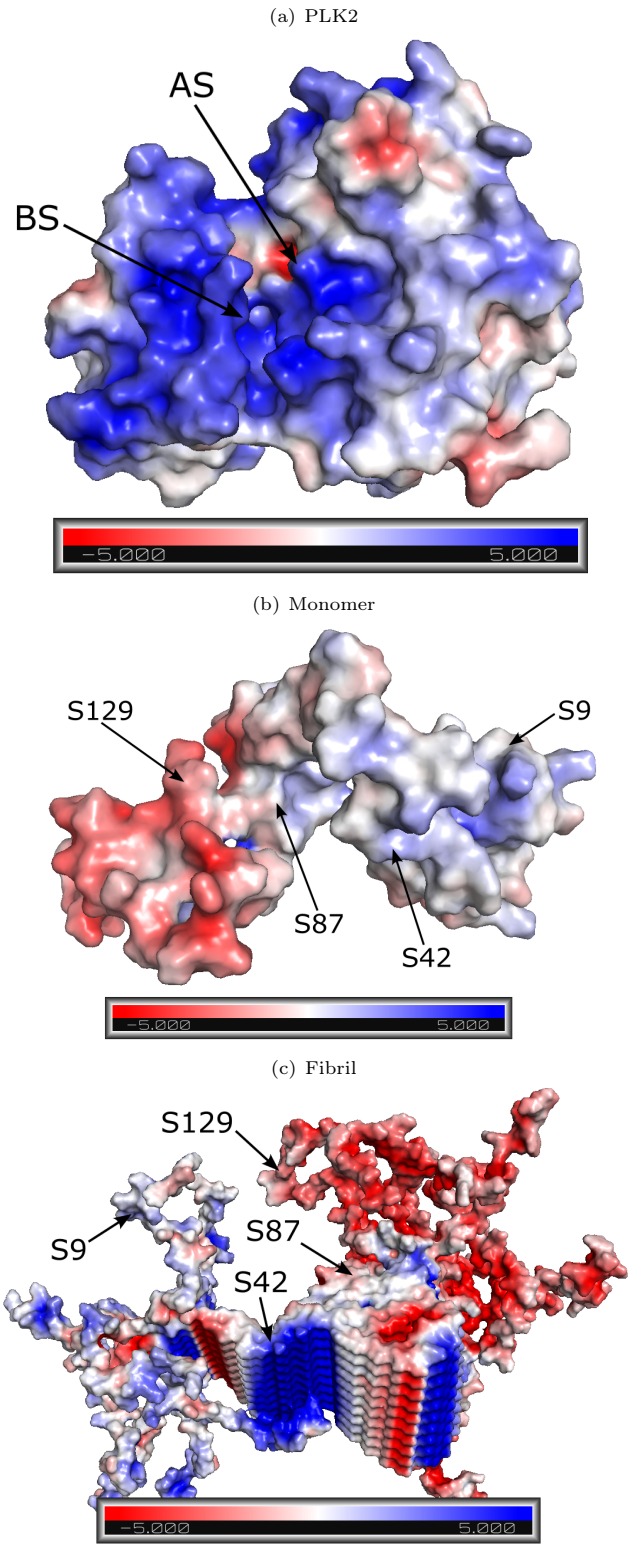

Figure 2. (a) PLK2[54] with indications for the binding site (BS) and active site (AS). Electrostatic potential of (b) the monomer and (c) fibrils[62] as calculated by the Poisson-Boltzmann equation with (b) all serine positions highlighted; or (c) the serine positions of the first protein in the fibril highlighted.

[7] The C-terminus – N-terminus distances experience large fluctuations, making this analysis not conclusive (Figure 14 in the SI).

Table 2. Calculated properties of AS and pAS. (i) Gyration (R_g) and hydrodynamic R_H radii of the entire proteins and of the NAC regions. The experimental value of R_H is 28.7 Å.[85] (ii) Average number of hydrogen bonds. (iii) Average number of salt bridges. Standard deviations are indicated in parenthesis.

	R_g [Å]	R_H [Å]	R_g(NAC) [Å]	R_H(NAC) [Å]	N_{HB}	N_{SB}
AS	35.6 (±12.8)	35.1 (±6.1)	23.8 (±16.4)	28.3(±11.3)	19.52 (±4.28)	1.54 (±1.23)
pAS	28.0 (±9.6)	31.0 (±5.8)	17.2(±9.2)	23.1 (±8.1)	20.67 (±4.32)	1.86 (±1.75)

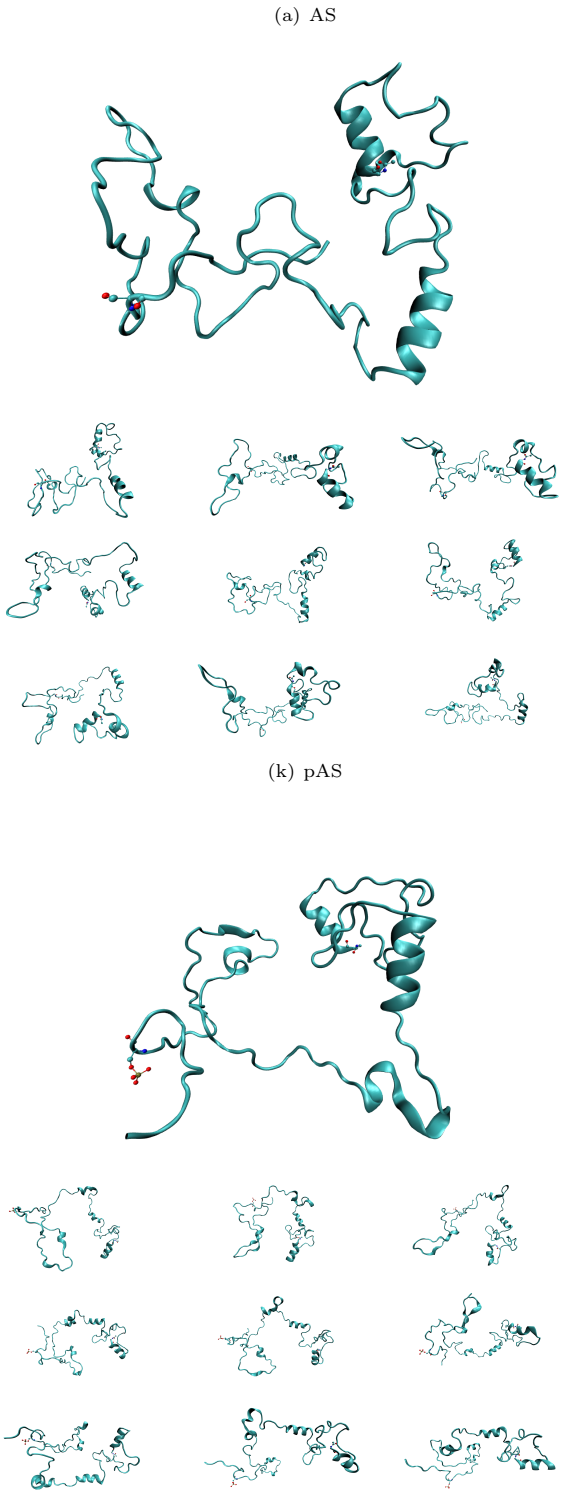

Figure 3. Representative structures of AS (a) and pAS (k) as determined by clustering. The acetyl group at the N-terminus and the residue at position S129 are shown as ball and sticks. The percentage of occurrence of the structures decreases from left to right and top to bottom (see Table 1 in the SI).

Table 3. Average solvent accessible surface areas (SASA) in AS and pAS in the NAC-Region and N- and C-terminus.

	SASA_N [nm^2]	SASA_{NAC} [nm^2]	SASA_C [nm^2]
AS	0.96 (±0.41)	0.87 (±0.31)	1.11 (±0.32)
pAS	0.90 (±0.42)	0.91 (±0.32)	1.13 (±0.39)

N-terminus. The phosphate group interacts to a small extent with sodium ions (Figure 21 in the SI) and, even less, with the protein residues (Figure 20 in the SI). In fact, the phosphate group is fully solvent exposed, as shown by a plot of the phosphate oxygen-water oxygen radial distribution functions (RDFs) (Figure 5). This might be caused, at least in part, by the absence of surrounding basic residues. However, one has to take into account also that current force field may lead to a overestimation of the number of interacting water molecules (See SI) This effect is even larger with the standard a99SB-*disp* force field (See SI). Within these caveats, we suggest that the electrostatic field of the phosphate is strongly reduced by its solvation and largely does not impact the C-terminus-N-terminus interactions. This lack of interaction may also in part be explained by AS containing no arginine residues that are known to interact strongly with phosphate groups,[87] yet none of the lysine residues present in the N-terminal domain formed salt bridges with S129 during the simulation (see Figure 3(a)).

The scenario of S129 in AS is dramatically different: the side chain does interact with the solvent at much lower rate. The Oγ atom has only 2 water hydrogen (Figure 5) and no sodium ions in its surrounding. The serine oxydril group forms instead a variety of *intramolecular* H-bonds (with K80, K96, K97 , K102, E126, E130 and E131 (Figure 20 in the SI).[8]

The serine in AS is instead involved in intermolecular contacts and, indeed AS features a larger number of the latter relative to pAS. In addition, The electrostatic interactions with the rest of the protein may be screened by the presence of positively charged counterions.

Analysis of the fibrils. The PTM introduces additional negative charges far from basic residues as observed in the monomeric form: K6 is the closest basic residue, located at 2.39 nm from S129. This residue is expected to fully solvated, in contrast to the NAC region.[62] At the speculative level, we may expect that water and counterions (absent in the structure[62]) may stabilize the phosphate group similarly to what observed for the monomer.

4. Conclusions. Here, we investigated the effects of phosphorylation on the structural ensemble of AS in solution in fibrillar forms. The residue is selected to be phosphorylated by its cognate kinase enzyme in a negatively charge region such as the C-term (both in solution and in the fibrils), because of its high positive potential. Once phosphorylated, the AS monomer does not undergo very large con-

[8] S129 backbone units interact with the solvent and nearby protein hydrogens in both AS and pAS.

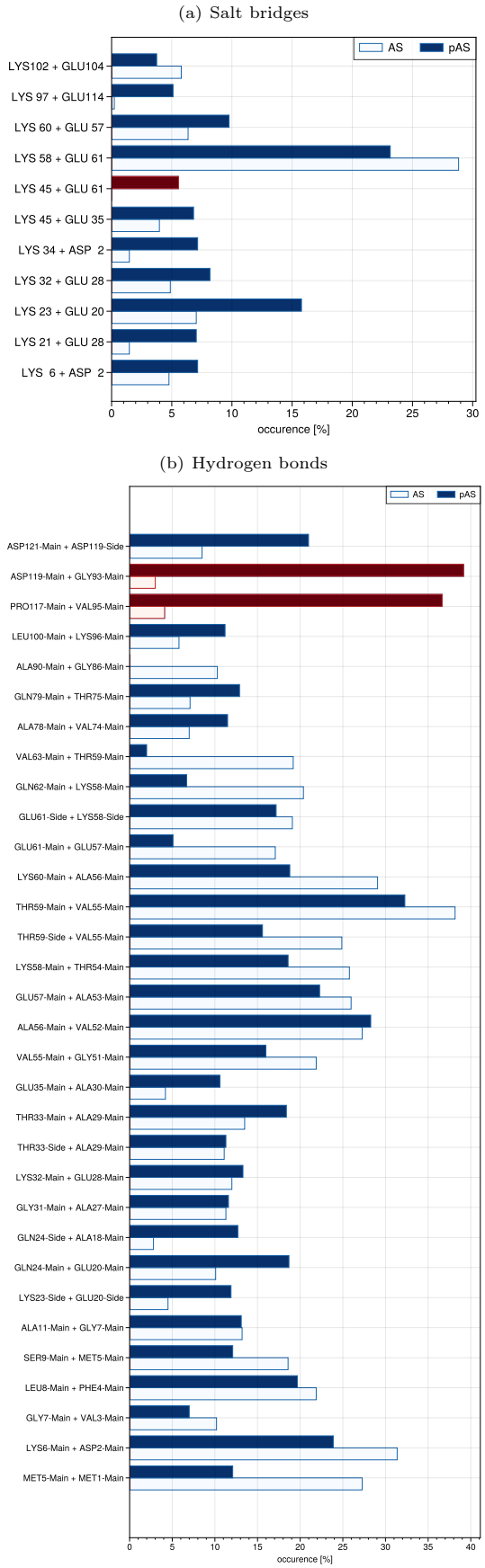

Figure 4. Occurence of intradomain (blue) and interdomain (red)) salt bridges (a) and H-bonds (b) in AS and pAS.

formational changes, becoming slightly more compact than the unmodified protein. The effect size may be ascribed to the fact that the added phosphate moiety points towards the solvent (within the limitations of the force field), and interacts, to a lesser extent, with counterions. Our calculations are consistent with the fact that CD spectra do not change significantly upon S129 phosphorylation in the unacetylated protein.[86] As the overall helicity in AS is low, the sensitivity of the calculated CD spectra may not be sufficient to register any changes in pAS that are small in terms of overall secondary structure, yet large when compared to AS. Addition caution must also be exerted when comparing results from unacetylated AS and physiological AS.[17] Finally, in the fibrils, the phosphate moiety might be solvated and stabilized by counterions, similarly to what we observed in aqueous solution for the monomer.

Acknowledgement TFO is supported by DFG (SFB1286-B8) and under Germany's Excellence Strategy - EXC 2067/1- 390729940. This work was partially performed as part of the Helmholtz School for Data Science in Life, Earth and Energy (HDS-LEE) and received funding from the Helmholtz Association of German Research Centers. Open Access publication funded by the Deutsche Forschungsgemeinschaft (DFG, German Research Foundation) – 491111487. The authors gratefully acknowledge the Gauss Centre for Supercomputing e.V. (www.gauss-centre.eu) for funding this project by providing computing time through the John von Neumann Institute for Computing (NIC) on the GCS Supercomputer JUWELS at Jülich Supercomputing Centre (JSC).[88–91]

References

(1) Hou, Y.; Dan, X.; Babbar, M.; Wei, Y.; Hasselbalch, S. G.; Croteau, D. L.; Bohr, V. A. Ageing as a risk factor for neurodegenerative disease. *Nature Reviews Neurology* **2019**, *15*, 565–581.

(2) Rocca, W. A. The burden of Parkinson's disease: a worldwide perspective. *The Lancet* **2018**, *17*, 928–929.

(3) Lücking, C. B.; Brice, A. Alpha-synuclein and Parkinson's disease. *Cellular and Molecular Life Sciences CMLS* **2000**, *57*, 1894–1908.

(4) Baba, M.; Nakajo, S.; Tu, P.-H.; Tomita, T.; Nakaya, K.; Lee, V.; Trojanowski, J. Q.; Iwatsubo, T. Aggregation of alpha-synuclein in Lewy bodies of sporadic Parkinson's disease and dementia with Lewy bodies. *The American journal of pathology* **1998**, *152*, 879–884.

(5) Gibb, W.; Lees, A. The relevance of the Lewy body to the pathogenesis of idiopathic Parkinson's disease. *Journal of Neurology, Neurosurgery & Psychiatry* **1988**, *51*, 745–752.

(6) Nguyen, P. H.; Ramamoorthy, A.; Sahoo, B. R.; Zheng, J.; Faller, P.; Straub, J. E.; Dominguez, L.; Shea, J.-E.; Dokholyan, N. V.; De Simone, A., et al. Amyloid oligomers: A joint experimental/computational perspective on Alzheimer's disease, Parkinson's disease, type II diabetes, and amyotrophic lateral sclerosis. *Chemical reviews* **2021**, *121*, 2545–2647.

(7) Waudby, C. A.; Camilloni, C.; Fitzpatrick, A. W.; Cabrita, L. D.; Dobson, C. M.; Vendruscolo, M.; Christodoulou, J. In-cell NMR characterization of the secondary structure populations of a disordered conformation of α-synuclein within E. coli cells. *PloS one* **2013**, *8*, e72286.

(8) Snead, D.; Eliezer, D. Alpha-synuclein function and dysfunction on cellular membranes. *Experimental neurobiology* **2014**, *23*, 292.

(9) Ghanem, S. S.; Majbour, N. K.; Vaikath, N. N.; Ardah, M. T.; Erskine, D.; Jensen, N. M.; Fayyad, M.; Sudhakaran, I. P.; Vasili, E.; Melachroinou, K., et al. α-Synuclein phosphorylation at serine 129 occurs after initial protein deposition and inhibits seeded fibril formation and toxicity. *Proceedings of the National Academy of Sciences* **2022**, *119*, e2109617119.

(10) Wang, Y.; Shi, M.; Chung, K. A.; Zabetian, C. P.; Leverenz, J. B.; Berg, D.; Srulijes, K.; Trojanowski, J. Q.; Lee, V. M.-Y.; Siderowf, A. D., et al. Phosphorylated α-synuclein in Parkinson's disease. *Science translational medicine* **2012**, *4*, 121ra20–121ra20.

(11) Kawahata, I.; Finkelstein, D. I.; Fukunaga, K. Pathogenic Impact of α-Synuclein Phosphorylation and Its Kinases in α-Synucleinopathies. *International Journal of Molecular Sciences* **2022**, *23*, 6216.

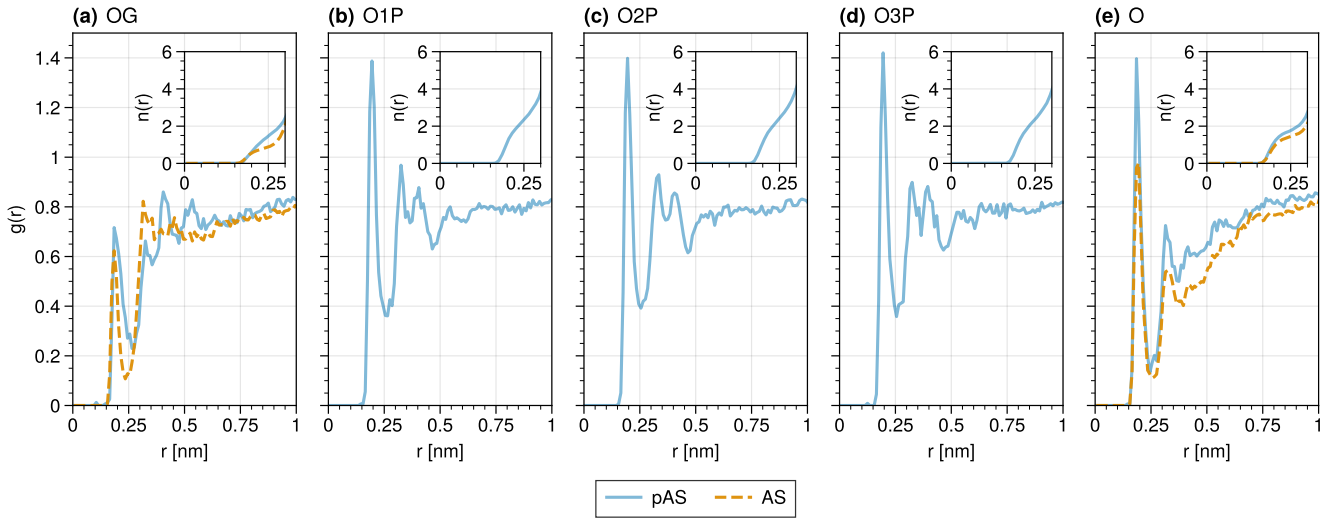

Figure 5. RDF ($g(r)$) of the oxygen atoms of residue 129 and water hydrogens (a-e). Compare the RDF for pAS (blue) and AS (orange) for the oxygen atom in the sidechain (a) and the carbonyl oxygen (e). (b)-(d) illustrate the RDF for the terminal phosphoryl oxygens. Insets show the integral of $g(r)$ up to 0.3 nm.

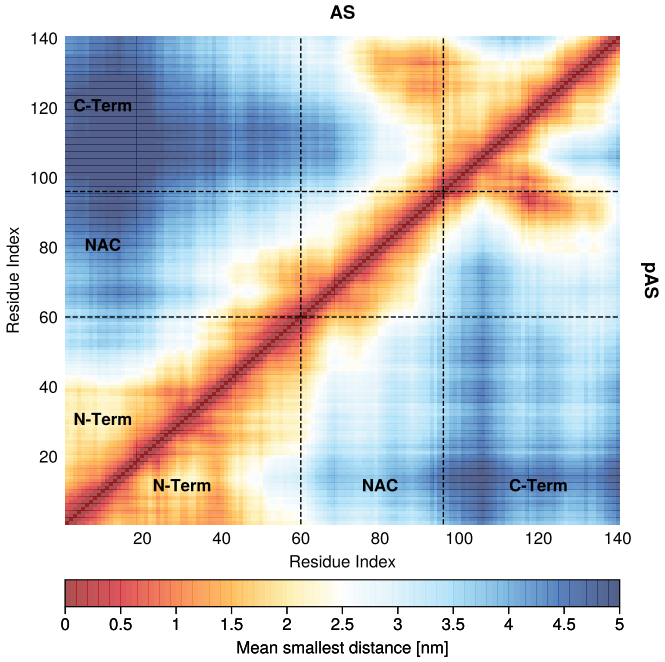

Figure 6. Contact maps in AS (triangle above) and pAS (triangle below).

(12) Xie, Y.; Jiang, Y.; Ben-Amotz, D. Detection of amino acid and peptide phosphate protonation using Raman spectroscopy. *Analytical biochemistry* **2005**, *343*, 223–230.

(13) Paleologou, K. E.; Schmid, A. W.; Rospigliosi, C. C.; Kim, H.-Y.; Lamberto, G. R.; Fredenburg, R. A.; Lansbury, P. T.; Fernandez, C. O.; Eliezer, D.; Zweckstetter, M., et al. Phosphorylation at Ser-129 but not the phosphomimics S129E/D inhibits the fibrillation of α-synuclein. *Journal of Biological Chemistry* **2008**, *283*, 16895–16905.

(14) Schreurs, S.; Gerard, M.; Derua, R.; Waelkens, E.; Taymans, J.-M.; Baekelandt, V.; Engelborghs, Y. In vitro phosphorylation does not influence the aggregation kinetics of WT α-synuclein in contrast to its phosphorylation mutants. *International journal of molecular sciences* **2014**, *15*, 1040–1067.

(15) Braithwaite, S. P.; Stock, J. B.; Mouradian, M. M. α-Synuclein phosphorylation as a therapeutic target in Parkinson's disease. *Reviews in the Neurosciences* **2012**, *23*, 191–198.

(16) Wang, L.; Friesner, R. A.; Berne, B. Replica exchange with solute scaling: a more efficient version of replica exchange with solute tempering (REST2). *The Journal of Physical Chemistry B* **2011**, *115*, 9431–9438.

(17) Rossetti, G.; Musiani, F.; Abad, E.; Dibenedetto, D.; Mouhib, H.; Fernandez, C. O.; Carloni, P. Conformational ensemble of human α-synuclein physiological form predicted by molecular simulations. *Physical Chemistry Chemical Physics* **2016**, *18*, 5702–5706.

(18) Palomino-Hernandez, O.; Buratti, F. A.; Sacco, P. S.; Rossetti, G.; Carloni, P.; Fernandez, C. O. Role of Tyr-39 for the Structural Features of α-Synuclein and for the Interaction with a Strong Modulator of Its Amyloid Assembly. *International journal of molecular sciences* **2020**, *21*, 5061.

(19) Theillet, F.-X.; Binolfi, A.; Bekei, B.; Martorana, A.; Rose, H. M.; Stuiver, M.; Verzini, S.; Lorenz, D.; Van Rossum, M.; Goldfarb, D., et al. Structural disorder of monomeric α-synuclein persists in mammalian cells. *Nature* **2016**, *530*, 45–50.

(20) Robustelli, P.; Piana, S.; Shaw, D. E. Developing a molecular dynamics force field for both folded and disordered protein states. *Proceedings of the National Academy of Sciences* **2018**, *115*, E4758–E4766.

(21) Robustelli, P.; Ibanez-de Opakua, A.; Campbell-Bezat, C.; Giordanetto, F.; Becker, S.; Zweckstetter, M.; Pan, A. C.; Shaw, D. E. Molecular basis of small-molecule binding to α-synuclein. *bioRxiv* **2021**,

(22) Uluca, B.; Viennet, T.; Petrović, D.; Shaykhalishahi, H.; Weirich, F.; Gönülalan, A.; Strodel, B.; Etzkorn, M.; Hoyer, W.; Heise, H. DNP-enhanced MAS NMR: a tool to snapshot conformational ensembles of α-synuclein in different states. *Biophysical journal* **2018**, *114*, 1614–1623.

(23) Jain, K.; Ghribi, O.; Delhommelle, J. Folding free-energy landscape of α-synuclein (35–97) via replica exchange molecular dynamics. *Journal of Chemical Information and Modeling* **2020**, *61*, 432–443.

(24) Ilie, I. M.; Nayar, D.; Den Otter, W. K.; Van Der Vegt, N. F.; Briels, W. J. Intrinsic conformational preferences and interactions in α-synuclein fibrils: insights from molecular dynamics simulations. *Journal of chemical theory and computation* **2018**, *14*, 3298–3310.

(25) Chwastyk, M.; Cieplak, M. Conformational biases of α-synuclein and formation of transient knots. *The Journal of*

Physical Chemistry B **2019**, *124*, 11–19.
(26) Perlmutter, J. D.; Braun, A. R.; Sachs, J. N. Curvature dynamics of α-synuclein familial parkinson disease mutants. *Journal of Biological Chemistry* **2009**, *284*, 7177–7189.
(27) Allison, J. R.; Varnai, P.; Dobson, C. M.; Vendruscolo, M. Determination of the free energy landscape of α-synuclein using spin label nuclear magnetic resonance measurements. *Journal of the American Chemical Society* **2009**, *131*, 18314–18326.
(28) Amos, S.-B. T.; Schwarz, T. C.; Shi, J.; Cossins, B. P.; Baker, T. S.; Taylor, R. J.; Konrat, R.; Sansom, M. S. Membrane Interactions of α-Synuclein Revealed by Multiscale Molecular Dynamics Simulations, Markov State Models, and NMR. *The Journal of Physical Chemistry B* **2021**, *125*, 2929–2941.
(29) Herrera, F. E.; Chesi, A.; Paleologou, K. E.; Schmid, A.; Munoz, A.; Vendruscolo, M.; Gustincich, S.; Lashuel, H. A.; Carloni, P. Inhibition of α-synuclein fibrillization by dopamine is mediated by interactions with five C-terminal residues and with E83 in the NAC region. *PloS one* **2008**, *3*, e3394.
(30) Robustelli, P.; Ibanez-de Opakua, A.; Campbell-Bezat, C.; Giordanetto, F.; Becker, S.; Zweckstetter, M.; Pan, A. C.; Shaw, D. E. Molecular basis of small-molecule binding to α-synuclein. *Journal of the American Chemical Society* **2022**, *144*, 2501–2510.
(31) Balesh, D.; Ramjan, Z., et al. Unfolded annealing molecular dynamics conformers for wild-type and disease-associated variants of alpha-synuclein show no propensity for beta-sheetformation. *Journal of Biophysical Chemistry* **2011**, *2011*.
(32) Allison, J. R.; Rivers, R. C.; Christodoulou, J. C.; Vendruscolo, M.; Dobson, C. M. A relationship between the transient structure in the monomeric state and the aggregation propensities of α-synuclein and β-synuclein. *Biochemistry* **2014**, *53*, 7170–7183.
(33) Dedmon, M. M.; Lindorff-Larsen, K.; Christodoulou, J.; Vendruscolo, M.; Dobson, C. M. Mapping long-range interactions in α-synuclein using spin-label NMR and ensemble molecular dynamics simulations. *Journal of the American Chemical Society* **2005**, *127*, 476–477.
(34) Park, S.; Yoon, J.; Jang, S.; Lee, K.; Shin, S. The role of the acidic domain of α-synuclein in amyloid fibril formation: a molecular dynamics study. *Journal of Biomolecular Structure and Dynamics* **2016**, *34*, 376–383.
(35) Brodie, N. I.; Popov, K. I.; Petrotchenko, E. V.; Dokholyan, N. V.; Borchers, C. H. Conformational ensemble of native α-synuclein in solution as determined by short-distance crosslinking constraint-guided discrete molecular dynamics simulations. *PLoS computational biology* **2019**, *15*, e1006859.
(36) Tsigelny, I. F.; Bar-On, P.; Sharikov, Y.; Crews, L.; Hashimoto, M.; Miller, M. A.; Keller, S. H.; Platoshyn, O.; Yuan, J. X.-J.; Masliah, E. Dynamics of α-synuclein aggregation and inhibition of pore-like oligomer development by β-synuclein. *The FEBS journal* **2007**, *274*, 1862–1877.
(37) Ramis, R.; Ortega-Castro, J.; Casasnovas, R.; Mariño, L.; Vilanova, B.; Adrover, M.; Frau, J. A coarse-grained molecular dynamics approach to the study of the intrinsically disordered protein α-synuclein. *Journal of chemical information and modeling* **2019**, *59*, 1458–1471.
(38) Yu, H.; Han, W.; Ma, W.; Schulten, K. Transient β-hairpin formation in α-synuclein monomer revealed by coarse-grained molecular dynamics simulation. *The Journal of chemical physics* **2015**, *143*, 12B623_1.
(39) Narayanan, C.; Weinstock, D. S.; Wu, K.-P.; Baum, J.; Levy, R. M. Investigation of the polymeric properties of α-synuclein and comparison with NMR experiments: a replica exchange molecular dynamics study. *Journal of chemical theory and computation* **2012**, *8*, 3929–3942.
(40) Dibenedetto, D.; Rossetti, G.; Caliandro, R.; Carloni, P. A molecular dynamics simulation-based interpretation of nuclear magnetic resonance multidimensional heteronuclear spectra of α-synuclein· dopamine adducts. *Biochemistry* **2013**, *52*, 6672–6683.
(41) Tsigelny, I. F.; Sharikov, Y.; Miller, M. A.; Masliah, E. Mechanism of alpha-synuclein oligomerization and membrane interaction: theoretical approach to unstructured proteins studies. *Nanomedicine: Nanotechnology, Biology and Medicine* **2008**, *4*, 350–357.
(42) Zhang, T.; Tian, Y.; Li, Z.; Liu, S.; Hu, X.; Yang, Z.; Ling, X.; Liu, S.; Zhang, J. Molecular dynamics study to investigate the dimeric structure of the full-length α-synuclein in aqueous solution. *Journal of Chemical Information and Modeling* **2017**, *57*, 2281–2293.
(43) Piana, S.; Robustelli, P.; Tan, D.; Chen, S.; Shaw, D. E. Development of a force field for the simulation of single-chain proteins and protein–protein complexes. *Journal of chemical theory and computation* **2020**, *16*, 2494–2507.
(44) Pedersen, K. B.; Flores-Canales, J. C.; Schiøtt, B. Predicting molecular properties of α-synuclein using force fields for intrinsically disordered proteins. *Proteins: Structure, Function, and Bioinformatics* **2023**, *91*, 47–61.
(45) Khoury, G. A.; Thompson, J. P.; Smadbeck, J.; Kieslich, C. A.; Floudas, C. A. Forcefield_PTM: Ab initio charge and AMBER forcefield parameters for frequently occurring post-translational modifications. *Journal of chemical theory and computation* **2013**, *9*, 5653–5674.
(46) Petrov, D.; Margreitter, C.; Grandits, M.; Oostenbrink, C.; Zagrovic, B. A systematic framework for molecular dynamics simulations of protein post-translational modifications. *PLoS computational biology* **2013**, *9*, e1003154.
(47) Zhong, B.; Song, G.; Chen, H.-F. Balanced Force Field ff03CMAP Improving the Dynamics Conformation Sampling of Phosphorylation Site. *International Journal of Molecular Sciences* **2022**, *23*, 11285.
(48) Margreitter, C.; Reif, M. M.; Oostenbrink, C. Update on phosphate and charged post-translationally modified amino acid parameters in the GROMOS force field. *Journal of computational chemistry* **2017**, *38*, 714–720.
(49) Vymětal, J.; Jurásková, V.; Vondrášek, J. AMBER and CHARMM force fields inconsistently portray the microscopic details of phosphorylation. *Journal of Chemical Theory and Computation* **2018**, *15*, 665–679.
(50) Rieloff, E.; Skepö, M. Phosphorylation of a disordered peptide—Structural effects and force field inconsistencies. *Journal of chemical theory and computation* **2020**, *16*, 1924–1935.
(51) Steinbrecher, T.; Latzer, J.; Case, D. Revised AMBER parameters for bioorganic phosphates. *Journal of chemical theory and computation* **2012**, *8*, 4405–4412.
(52) Tucker, M. R.; Piana, S.; Tan, D.; LeVine, M. V.; Shaw, D. E. Development of Force Field Parameters for the Simulation of Single- and Double-Stranded Dna Molecules and Dna-Protein Complexes. *The Journal of Physical Chemistry B* **2022**, *126*, 4442–4457.
(53) Berman, H. M.; Westbrook, J.; Feng, Z.; Gilliland, G.; Bhat, T. N.; Weissig, H.; Shindyalov, I. N.; Bourne, P. E. The protein data bank. *Nucleic acids research* **2000**, *28*, 235–242.
(54) Aubele, D. L.; Hom, R. K.; Adler, M.; Galemmo Jr, R. A.; Bowers, S.; Truong, A. P.; Pan, H.; Beroza, P.; Neitz, R. J.; Yao, N., et al. Selective and brain-Permeable Polo-like Kinase-2 (Plk-2) inhibitors that reduce α-synuclein phosphorylation in rat brain. *ChemMedChem* **2013**, *8*, 1295–1313.
(55) Long, A.; Zhao, H.; Huang, X. Structural basis for the interaction between casein kinase 1 delta and a potent and selective inhibitor. *Journal of Medicinal Chemistry* **2012**, *55*, 956–960.
(56) Pechkova, E.; Zanotti, G.; Nicolini, C. Three-dimensional atomic structure of a catalytic subunit mutant of human protein kinase CK2. *Acta Crystallographica Section D: Biological Crystallography* **2003**, *59*, 2133–2139.
(57) Komolov, K. E.; Bhardwaj, A.; Benovic, J. L. Atomic structure of G protein-coupled receptor kinase 5 (GRK5) reveals distinct structural features novel for GRKs. *J Biol Chem* **2015**, *290*, 20629–20647.
(58) Deniston, C.; Salogiannis, J.; Mathea, S.; Snead, D.; Lahiri, I.; Matyszewski, M.; Donosa, O.; Watanabe, R.; Böhning, J.; Shiau, A., et al. Structure of LRRK2 in Parkinson's disease and model for microtubule interaction. *Nature* **2020**, *588*, 344–349.
(59) Sigrist, C. J.; De Castro, E.; Cerutti, L.; Cuche, B. A.; Hulo, N.; Bridge, A.; Bougueleret, L.; Xenarios, I. New and continuing developments at PROSITE. *Nucleic acids research* **2012**, *41*, D344–D347.
(60) Sigrist, C. J.; Cerutti, L.; Hulo, N.; Gattiker, A.; Falquet, L.; Pagni, M.; Bairoch, A.; Bucher, P. PROSITE: a documented database using patterns and profiles as motif descriptors. *Briefings in bioinformatics* **2002**, *3*, 265–274.
(61) Sievers, F.; Wilm, A.; Dineen, D.; Gibson, T. J.; Karplus, K.; Li, W.; Lopez, R.; McWilliam, H.; Remmert, M.; Söding, J., et al. Fast, scalable generation of high-quality protein multiple sequence alignments using Clustal Omega. *Molecular systems biology* **2011**, *7*, 539.
(62) Tuttle, M. D.; Comellas, G.; Nieuwkoop, A. J.; Covell, D. J.; Berthold, D. A.; Kloepper, K. D.; Courtney, J. M.; Kim, J. K.; Barclay, A. M.; Kendall, A., et al. Solid-state NMR structure of a pathogenic fibril of full-length human α-synuclein. *Nature structural & molecular biology* **2016**, *23*, 409–415.
(63) Jurrus, E.; Engel, D.; Star, K.; Monson, K.; Brandi, J.; Felberg, L. E.; Brookes, D. H.; Wilson, L.; Chen, J.; Liles, K., et al. Improvements to the APBS biomolecular solvation software suite. *Protein Science* **2018**, *27*, 112–128.
(64) Schrödinger, LLC,
(65) DeLano, W. L., et al. Pymol: An open-source molecular graphics tool. *CCP4 Newsletter on protein crystallography* **2002**, *40*, 82–92.
(66) Darden, T.; York, D.; Pedersen, L. Particle mesh Ewald: An N log (N) method for Ewald sums in large systems. *The Journal of chemical physics* **1993**, *98*, 10089–10092.
(67) Evans, D. J.; Holian, B. L. The nose–hoover thermostat. *The Journal of chemical physics* **1985**, *83*, 4069–4074.
(68) Andersen, H. C. Molecular dynamics simulations at constant pressure and/or temperature. *The Journal of chemical physics* **1980**, *72*, 2384–2393.
(69) Hess, B.; Bekker, H.; Berendsen, H. J.; Fraaije, J. G. LINCS: a linear constraint solver for molecular simulations. *Journal of computational chemistry* **1997**, *18*, 1463–1472.
(70) Van Der Spoel, D.; Lindahl, E.; Hess, B.; Groenhof, G.; Mark, A. E.; Berendsen, H. J. GROMACS: fast, flexible, and free. *Journal of computational chemistry* **2005**, *26*, 1701–1718.
(71) Daura, X.; Gademann, K.; Jaun, B.; Seebach, D.; Van Gunsteren, W. F.; Mark, A. E. Peptide folding: when simulation meets experiment. *Angewandte Chemie International Edition* **1999**, *38*, 236–240.

(72) Han, B.; Liu, Y.; Ginzinger, S. W.; Wishart, D. S. SHIFTX2: significantly improved protein chemical shift prediction. *Journal of biomolecular NMR* **2011**, *50*, 43–57.
(73) McGibbon, R. T.; Beauchamp, K. A.; Harrigan, M. P.; Klein, C.; Swails, J. M.; Hernández, C. X.; Schwantes, C. R.; Wang, L.-P.; Lane, T. J.; Pande, V. S. MDTraj: A Modern Open Library for the Analysis of Molecular Dynamics Trajectories. *Biophysical Journal* **2015**, *109*, 1528 – 1532.
(74) Kabsch, W.; Sander, C. Dictionary of protein secondary structure: pattern recognition of hydrogen-bonded and geometrical features. *Biopolymers: Original Research on Biomolecules* **1983**, *22*, 2577–2637.
(75) Bulheller, B. M.; Hirst, J. D. DichroCalc—circular and linear dichroism online. *Bioinformatics* **2009**, *25*, 539–540.
(76) de Bruyn, E. SPEADI: Scalable Protein Environment Analysis for Dynamics and Ions (v1.0.0). 2022; `https://doi.org/10.5281/zenodo.7436713`.
(77) Humphrey, W.; Dalke, A.; Schulten, K. VMD: visual molecular dynamics. *Journal of molecular graphics* **1996**, *14*, 33–38.
(78) Mbefo, M. K.; Paleologou, K. E.; Boucharaba, A.; Oueslati, A.; Schell, H.; Fournier, M.; Olschewski, D.; Yin, G.; Zweckstetter, M.; Masliah, E., et al. Phosphorylation of synucleins by members of the Polo-like kinase family. *Journal of Biological Chemistry* **2010**, *285*, 2807–2822.
(79) Inglis, K. J.; Chereau, D.; Brigham, E. F.; Chiou, S.-S.; Schöebel, S.; Frigon, N. L.; Yu, M.; Caccavello, R. J.; Nelson, S.; Motter, R., et al. Polo-like kinase 2 (PLK2) phosphorylates α-synuclein at serine 129 in central nervous system. *Journal of Biological Chemistry* **2009**, *284*, 2598–2602.
(80) Chen, M.; Yang, W.; Li, X.; Li, X.; Wang, P.; Yue, F.; Yang, H.; Chan, P.; Yu, S. Age-and brain region-dependent α-synuclein oligomerization is attributed to alterations in intrinsic enzymes regulating α-synuclein phosphorylation in aging monkey brains. *Oncotarget* **2016**, *7*, 8466.
(81) Lowery, D. M.; Lim, D.; Yaffe, M. B. Structure and function of Polo-like kinases. *Oncogene* **2005**, *24*, 248–259.
(82) Paleologou, K. E.; Oueslati, A.; Shakked, G.; Rospigliosi, C. C.; Kim, H.-Y.; Lamberto, G. R.; Fernandez, C. O.; Schmid, A.; Chegini, F.; Gai, W. P., et al. Phosphorylation at S87 is enhanced in synucleinopathies, inhibits α-synuclein oligomerization, and influences synuclein-membrane interactions. *Journal of Neuroscience* **2010**, *30*, 3184–3198.
(83) Lazar, T.; Guharoy, M.; Vranken, W.; Rauscher, S.; Wodak, S. J.; Tompa, P. Distance-Based metrics for comparing conformational ensembles of intrinsically disordered proteins. *Biophysical Journal* **2020**, *118*, 2952–2965.
(84) Roche, J.; Ying, J.; Maltsev, A. S.; Bax, A. Impact of Hydrostatic Pressure on an Intrinsically Disordered Protein: A High-Pressure NMR Study of α-Synuclein. *ChemBioChem* **2013**, *14*, 1754–1761.
(85) Maltsev, A. S.; Ying, J.; Bax, A. Impact of N-terminal acetylation of α-synuclein on its random coil and lipid binding properties. *Biochemistry* **2012**, *51*, 5004–5013.
(86) Samuel, F.; Flavin, W. P.; Iqbal, S.; Pacelli, C.; Renganathan, S. D. S.; Trudeau, L.-E.; Campbell, E. M.; Fraser, P. E.; Tandon, A. Effects of serine 129 phosphorylation on α-synuclein aggregation, membrane association, and internalization. *Journal of Biological Chemistry* **2016**, *291*, 4374–4385.
(87) Mandel-Gutfreund, Y.; Schueler, O.; Margalit, H. Comprehensive Analysis of Hydrogen Bonds in Regulatory Protein Dna-Complexes: in Search of Common Principles. *Journal of Molecular Biology* **1995**, *253*, 370–382.
(88) Krause, D. Juwels: Modular Tier-0/1 Supercomputer At Jülich Supercomputing Centre. *Journal of large-scale research facilities JLSRF* **2019**, *5*, A135.
(89) Alvarez, D. Juwels Cluster and Booster: Exascale Pathfinder With Modular Supercomputing Architecture At Juelich Supercomputing Centre. *Journal of large-scale research facilities JLSRF* **2021**, *7*, A183.
(90) Herten, A. JUWELS Booster - Early User Experiences. Proceedings of the 2021 on Performance EngineeRing, Modelling, Analysis, and VisualizatiOn STrategy. 2021; p nil.
(91) Kesselheim, S. et al. *Lecture Notes in Computer Science*; Lecture Notes in Computer Science; Springer International Publishing, 2021; pp 453–468.